Smart Structures and Systems, 2017, Volume 20, Issue 6, pp. 669-682
DOI: 10.12989/sss.2017.20.6.669

A novel approach to damage localisation based on bispectral analysis and neural network

M. Civera[1 a], L. Zanotti Fragonara[2*], C. Surace[1 b]

[1]*Department of Structural, Building and Geotechnical engineering, Politecnico di Torino, Corso Duca degli Abruzzi, 24, Turin, 10129, Italy*

[2]*School of Aerospace, Transportation and Manufacturing, Cranfield University, College Road, Cranfield, MK43 0AL, United Kingdom*

(Received keep as blank , Revised keep as blank , Accepted keep as blank)9pt

Abstract. The normalised version of bispectrum, the so-called bicoherence, has often proved a reliable method of damage detection on engineering applications. Indeed, higher-order spectral analysis (HOSA) has the advantage of being able to detect non-linearity in the structural dynamic response while being insensitive to ambient vibrations. Skewness in the response may be easily spotted and related to damage conditions, as the majority of common faults and cracks shows bilinear effects.

The present study tries to extend the application of HOSA to damage localisation, resorting to a neural network based classification algorithm. In order to validate the approach, a non-linear finite element model of a 4-meters-long cantilever beam has been built. This model could be seen as a first generic concept of more complex structural systems, such as aircraft wings, wind turbine blades, etc.

The main aim of the study is to train a Neural Network (NN) able to classify different damage locations, when fed with bispectra. These are computed using the dynamic response of the FE nonlinear model to random noise excitation.

Keywords: structural health monitoring, damage detection, higher-order spectral analysis, bispectrum, neural network, non-linear vibrations, breathing crack.

1. Introduction

Structural Health Monitoring (SHM) using non-destructive, low-cost and reliable techniques has been one of the trending research areas because of the development in sensors and materials. Developing and implementing a functional and robust damage detection strategy has become a pivotal aim for researchers in the last decades. Techniques should be able to match a certain set of characteristics in order to be welcomed and applied widely, such as being fast in detection, non-destructive, global and automatic (Ciang, Lee, & Bang, 2008). Furthermore, they should be reliable and low-cost under service condition to be economically convenient, as SHM is intended to minimize time and cost of maintenance. Preventing unnecessary, expansive and in some cases even dangerous inspections while avoiding breakdowns or stops is the main goal of researchers in this field. Thus, another requirement is the ability to perform continuous monitoring of current situation, with constant sampling and updates.

In the last years, several authors explored a kaleidoscope of techniques to find the most suited ones. However, most of them are characterised by both pros and cons. Acoustic emission events detection methods (AE monitoring) proved to be very powerful for damage detection, but not as good for damage assessment (Ciang et al., 2008). Thermal imaging is a fast method, but also limited to near-to-surface defects and expensive, if, as in most cases, passive approach thermography is not possible and an external stimulus source is needed. Other methods such as ultrasonic investigations, X-radioscopy, Eddy currents or similar, are limited by being point-by-point techniques, useful only for local inspection.

Modal-based approaches have been the earliest to emerge and even now they remain the most common and used for damage detection (Boscato, Russo, Ceravolo, & Zanotti Fragonara, 2015; M. Civera, Surace, & Worden, 2017; Farrar & Worden, 2007). Indeed, they satisfy most of the aforementioned demands: being modal parameters functions of physical properties, a simple and global comparison between the current dynamic response and the expected one for the pristine structure can be performed at any given moment. In doing so, any change can be linked to damaged conditions. Thus a robust and reliable analysis procedure can be achieved by using cheap, simple and common sensor systems.

This paper is focused on bispectral analysis, that has already been applied successfully to different cases, like fixed offshore structures (A J Hillis & Courtney, 2011), concrete facilities (Xiang & Tso, 2002), cracks or similar (Chen, Hagiwara, Su, & Shi, 2002; Andrew J Hillis, Neild, Drinkwater, & Wilcox, 2006; Salawu, 1997). According to that, damage detection by using higher-order spectral

*Corresponding author, Lecturer,
E-mail: l.zanottifragonara@cranfield.ac.uk
[a] Ph.D. Student, E-mail: marco.civera@studenti.polito.it
[b] Professor, E-mail: cecilia.surace@polito.it

analysis (HOSA) can be definitively assumed as a reliable method and particularly suitable for the application, due to its insensitivity to white Gaussian noise (Akan & Ünsal Artan, 2003; Nikias & Mendel, 1993) and its tested ability to carry information even across difficult external conditions. (Roy, Kumar, & Bahl, 2002)

In spite of this, damage detection itself is not enough for SHM. Once defects have been spotted, further analyses about damage localisation, quantification and classification are required as forward steps of damage assessment. This work is thus focused on damage localisation as a method to improve the rapidity and precision of maintenance intervention after fault has been disclosed. Modal information has already been used in literature for damage localisation, but only considering local changes in modal stiffness or in modal mass (J.-T. Kim & Stubbs, 2002). Thus, this proposed method can hardly be applied to realistic cases in which natural noise could affect the processed signals.

In this paper, preliminary numerical validation on the capability of a new technique based on bispectrum to localise damage is presented. The simulations are based on a FE model of a 4-meters-long cantilever beam where a breathing crack has been placed in different positions. The technique has been validated using various white-noise excitations, supposed to be applied with a shaker close to the free extremity of the cantilever beam. The choice of a simple cantilever beam was done according to two main reasons. Firstly, this type of basic structure could be seen as a first generic concept of more complex structural systems, such as aircraft wings, wind turbine blades, etc. Secondly, FE models are always affected by imperfections and deviation from the real-world behaviour of modelled elements. These undesirable effects become more and more predominant and dangerous as the FE model becomes more complex. The cantilever beam is by default one of the safest choices when dealing with new approaches. Being the method validated on it, if the technique does not depend on a particular behaviour linked to its particular geometry there are no reasons to neglect a priori its extension to different, more complex structures.

In this study, white Gaussian noise has been chosen since it should maximise the detection capabilities of the bispectrum. Some early results were also reported in (Marco Civera, Zanotti Fragonara, & Surace, 2016); even if several improvements and slight changes on the approach have been implemented since then – as feature selection, for example – the basic idea suffered no changes. These enhancements increased substantially the capacity and the reliability of this novel method, which was already very promising.

Regarding the sort of damage investigated, “breathing” crack – also known as “opening” type of crack – can be seen as a functional representation of a broad range of damages due to fatigue. For this type of irregularities, the high sensitivity of vibration diagnostics, based on the use of non-linear effects, has already been proved in literature on beam-like structures (A. Bovsunovsky & Surace, 2015). Indeed, nonlinear distortions of vibrations recorded around super-harmonic and subharmonic resonances are seen as well-performing indicators of crack presence (Ruotolo, Surace, Crespo, & Storer, 1996) and have been applied extensively thenceforth (A. P. Bovsunovsky & Surace, 2005)(Pugno, Surace, & Ruotolo, 2000)(A. P. Bovsunovsky, Surace, & Bovsunovsky, 2006).

Several authors investigated the breathing crack problem resorting to different strategies in order to model the non-linear dynamics of the problem. For instance, some authors referred to plate/shell finite elements for studying the damaged cross-section (Chati, Rand, & Mukherjee, 1997) or to beam elements enriched of bilinear springs (Sundermeyer & Weaver, 1995). Solid- and beam- based models differ in terms of the number of elements used; both have been applied successfully to analyse the structural and dynamic behaviour of beams (Chandrashekhara & Bangera, 1993; Macneal & Harder, 1985; Michel, Hans, Guéguen, & Boutin, 2007). Solid models allow to focus on fissure real 3-D geometry (Gerstle, Martha, & Ingraffea, 1987; Martha, Wawrzynek, & Ingraffea, 1993), while modelling discontinuities as bilinear springs connecting pristine parts of the beam is widespread in dynamic state-of-the-art research (Kisa & Gurel, 2006). These devices are capable of carrying axial, shearing and bending effects, suitable for representing beams as one-dimensional continuum (Chondros, Dimarogonas, & Yao, 1998). However, a 3-D solid model with contact elements was preferred by the authors, due to their capacity of suiting the true geometry of the model and their documented reliability (Belytschko, Liu, Moran, & Elkhodary, 2013).

The dynamic response of the cantilever beam to the aforementioned Gaussian-distributed random noises has undergone the HOSA and the corresponding bispectra were thus computed. Then, by considering separately the various parts of these – real, imaginary, magnitude and phase, taken individually or paired, as will be explained deeper further on – a classification system based on neural network has been trained to localise the damage.

The paper is organized as follows: in Section 2 the theoretical background of Higher-Order Spectral Analysis is briefly discussed; in Section 3 the Finite Element model and the non-linear analyses carried out are described; in Section 4 obtained bispectra are shown and examined; in Section 5 the optimisation methodology for the neural network (NN)’s architecture and parameters is presented; in Section 6 the performance of the NN, with respect to the several option investigated, is reported and discussed, according to the various components of the bispectral data; in Section 7 the performance of the NN for some new cracks, located in positions not corresponding to any of the previous ones used for training, is also tested; finally in Section 8 the identified results of damage localisation will be interpreted and conclusions about them will be exposed.

2. Bispectral Analysis

The Bispectrum represents the two-dimensional Fourier transform of the second-order correlation function $C(\tau_1, \tau_2) = E[x(t)x(t+\tau_1)x(t+\tau_2)]$, where E denotes the expectation operator. In turn, this correlation function is

defined in terms of a third-order product moment. This leads the bispectrum itself to be a cubic (third-order) spectral density. Its most intuitive representation is in the frequency-domain, and is represented by equation (1):

$$B(f_1, f_2) = \lim_{T\to\infty} \frac{1}{T} E\left[X(f_1) X(f_2) X^*(f_1 + f_2) \right] \quad (1)$$

where B represents the bispectrum evaluated at the two frequencies f_1 and f_2, $X(f)$ is the Fourier transform of a generic process x(t) and the symbol * (asterisk) denotes complex conjugation. Thus, it can be seen as the product of these three spectral components. The bispectrum most notable ability is to provide information about the skewness (or asymmetry) of a given process, whereas power spectra (that is, second-order cumulants) are "phase-blind" and can only describe linear mechanisms. The bispectrum was firstly introduced for signal processing in the field of wave-wave interaction, by (Y. C. Kim & Powers, 1978).

Ideally, the bispectrum returns non-zero values when *phase coherence* – due to any sort of nonlinear or parametric interaction – exists in a continuous spectrum (Greb & Rusbridge, 2000). In fact, the purpose of its very first use was to discriminate between nonlinear interactions and spontaneously excited independent modes by estimating the degree of phase coherence between them. To cite Kim & Powers' own example, given three waves defined by their frequencies (ω_1, ω_2, ω_3) and wavenumbers (k_1, k_2, k_3), the resonance conditions are (a) $\omega_1 + \omega_2 = \omega_3$ and (b) $k_1 + k_2 = k_3$. If ω_3 happens to be a normal mode of the system, the selections rules (a) and (b) become no longer sufficient to implicate that the presence of a wave with this frequency is the results of some nonlinearities, as it can be simply excited on its own for reasons not linked to ω_1 and ω_2. However, phase coherence (also known as *phase consistency*) comes in useful in these circumstances, as if ω_3 would be independent from the other two frequencies, it should be characterised by a statistically independent random phase. Because of that, statistical averaging through expected value operator E[·] will return a zero value. If not – i.e., if a phase coherence does exist as $\phi_1 + \phi_2 = \phi_3$) – the so-defined Bispectrum will have a non-null value. In that latter case, the option of a spontaneously excited independent mode can be reasonably rejected.

Moreover, bispectra do not only carry information about deviation from Gaussian normal distribution, but can also be used to properly get insight about the nonlinear mechanisms that govern the analysed system and to esteem the phase of its recorded response signal. A detailed explication of these two aspects can be found in the work of (Niakis & Raghuveer, 1987). Thus, use of bispectral analysis can lead to Nonlinear System Identification (NLSI), which still remains one of the most challenging issues for the current state of research in the field of structural mechanics.

For what concerns damage detection, the principle is that a crack behaves nonlinearly under an applied driving force; in fact, it is well known that the opening and closing of the crack under forced vibration results in generation of super-harmonics. For damage detection alone, bicoherence should be preferred over bispectrum, as it is a more synthetic index of non-linearity, being it a normalised version of the latter, though some authors refer to the bispectrum even for damage detection (Andrew J Hillis et al., 2006). A deeper explanation of bicoherence and of its role in damage detection can be found in the work of Collis et al (Collis, White, & Hammond, 1998).

In this work, the damage localisation properties of the bispectrum are to be investigated. For damage localisation the bicoherence is considered to be unsuitable, because a scalar value alone results to be insufficient information to work with properly. Indeed, in order to locate the crack position correctly, phase coupling and relative levels of the different super-harmonics are expected to play different roles when cracks are moving closer or farther from the investigated position.

Another great advantage of using bispectral analysis is its insensitivity to uncorrelated random noise. That is simply explained by the fact that all Gaussian distribution will have zero asymmetry and so null bispectrum. Being natural noise one of the most common threats to accuracy and reliability in simpler analysis, this aspect is extremely positive for any practical application. A more detailed dissertation about the theory behind higher-order spectral analysis can be found, for example, in the works of (Collis et al., 1998) and (Fackrell, 1995).

It should be remarked that, apart from what theory says, since bispectra are estimated with a finite number of data, Gaussian noise is not null and it may affect somehow the analysis performance. However, it is generally possible to assume its effects to be tolerable. Particularly, three artificially-generated signal-to-noise ratios (SNRs) have been used here (100, 50 and 20), in order to simulate real-life circumstances.

3. Non-Linear Finite Element Models

3.1 Reference FE models

A 4-meters-long cantilever beam with a single through crack, as shown in Figure 1, has been modelled in ANSYS Mechanical APDL®. The cross-section is defined as a 0.2 x 0.2 m square, while material properties are enlisted

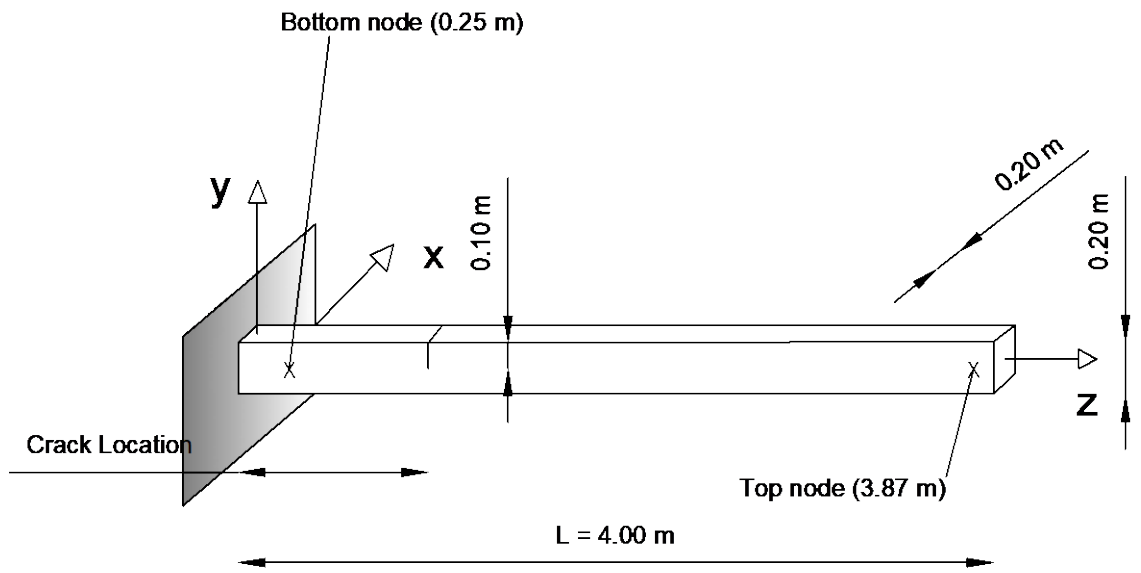

Fig. 1. Cantilever beam geometry (section 0.2 by 0.2 m, length 4 m) and the two measurements position. The extension of the cracks was assumed to be half the width of the beam. The nine crack locations are all spaced by 40 cm from each other and from the fixed and free ends.

hereinafter (material is assumed to be isotropic).

- E = 30 GPa Young's Modulus
- ν = 0.18 Poisson's Ratio
- ρ = 2300 kg/m^3 material density

The coordinate reference system is centred at the geometric barycentre of the restrained extremity and has the z-axis coincident with beam main direction, while the x- and y-axes are parallel to the cross-section sides.

The cantilever beam has been modelled using SOLID185 elements (8-noded prismatic solids). Each node has 3 degrees of freedom (DoFs), this meaning that it can translate along x-, y- and z-axes (displacements u_x, u_y and u_z respectively). The $\bar{B}$ -bar method (also known as *selective reduced integration method*) was selected, meaning that volumetric strain at Gauss integration points have been replaced with the average volumetric strain of the elements, to avoid locking problems. Even if this approach lacks the capacity to handle with shear locking in bending-dominated problems, in this case the cross-section of the model is absolutely not thin enough to justify a more complex option.

Different types of contacts have been investigated in order to find the best candidate for the transient non-linear dynamic simulations required. A surface-to-surface contact element was finally chosen, using the TARGET170 and CONTA174 ANSYS elements (3-dimensional, 8-noded surface-to-surface contact element) to model the breathing crack mechanism (see Figure 2). The default options of ANSYS were left untouched for the contact behaviour: isotropic Coulomb friction, augmented Lagrangian contact algorithm, contact detection point at Gauss nodes and bonded behaviour. The two surfaces representing the crack were set as in contact in the initial state of the system.

Geometrically, the crack was modelled as passing through the whole thickness of the element along x-axis (Figure 2). In this study, the crack thickness was not relevant, since, as aforementioned, the initial condition of the dynamic analysis is to set the two surfaces representing the crack in full contact. This assumption as already been proved to be trustable in literature (Surace, Ruotolo, & Storer, 2011). The crack surface spanned over half of the total cross-section area.

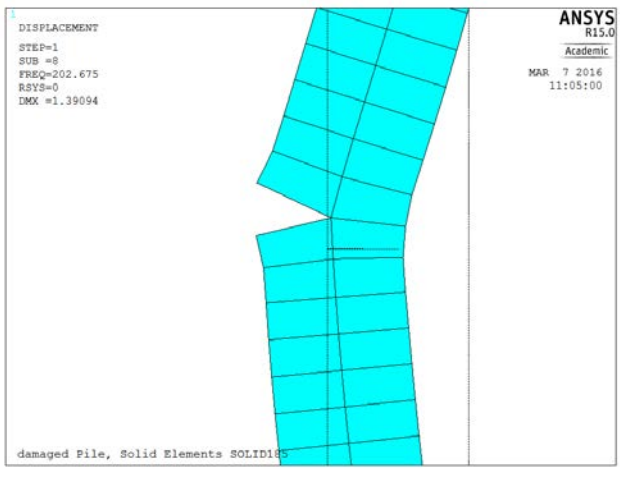

Figure 1. Breathing crack mechanism (crack open during modal analysis).
Displacement over-magnified for clarity's sake.

The crack location has been parameterised so to vary into nine different positions, all equally distant from each other, defined in steps of 40 centimetres along z-axis. Obtained results are listed on the following Table 1. Please

note that the natural frequencies values are coupled according to the symmetry of the structural element when the behaviour is linear. Analytical results (as shown for comparison) are calculated according to the solution for a simple cantilever beam:

$$\omega_n = (\chi_n L)^2 \sqrt{\frac{EI}{\bar{m}L^4}} \quad (2)$$

where $\chi_n L$ is a constant ratio and can be found consulting tables of hyperbolic and trigonometric functions (the first four are: 1.875, 4.694, 7.855, 10.996), E is the Young's Modulus, I is the moment of inertia, $\bar{m}$ is the mass for linear unit along z-axis (referring to Figure 1) and L is the total length of the beam. For what concerns the n-*th* axial and the first torsional mode, they can be computed with the following equations:

$$\omega_{n,axial} = \frac{2n-1}{2}\pi\sqrt{\frac{EA}{\bar{m}L^2}} \quad (3)$$

$$\omega_{1,torsional} = 2\pi\sqrt{\frac{3GI_t}{\rho J_p L^2}} \quad (4)$$

where the torsional frequency has been computed in the assumption of a linear mode shape with the Rayleigh method. Inside the equation, G is the Shear Modulus, I_t the torsional stiffness (computed as $I_t = \beta a b^3$, where $\beta = \frac{1}{7.1}$), J_p the moment of polar inertia and ρ is the density. ANSYS solves the eigenvalue problem for the damaged structure assuming the crack is always opened.

Table 1 Modal Analysis results on pristine (undamaged) cantilever beam. All bending modes occur at the same frequency along both directions (x and y axes).

	Classification	Analytical [Hz]	ANSYS [Hz]
1	1st bending	7.31	7.06
2	2nd bending	45.83	43.83
3	3rd bending	124.25	121.07
4	1st torsional	132.09	146.94
5	1st axial	225.84	225.87
6	4th bending	251.52	232.77

3.2 Non-linear time history analyses with Gaussian white noise as excitation source.

In order to produce a dataset to train the neural network, a series of full-transient, non-linear, time-history analyses have been run on the cracked model in ANSYS. The sampling time has been defined according to the Nyquist criterion for the 1st natural frequency. Since the quality of the results will strongly depend on the super-harmonics contained in the response, frequency up to the third harmonic for the first mode are to be measured. This introduces some limits on the sampling time according to (Bathe, 2005), which has to be set to a value corresponding to 1/20 T_u, where $T_u = 2\pi/\omega_u$ (and ω_u is the highest frequency in the input load). Thus, in order to properly investigate frequencies and harmonics up to 50 Hz the sampling time was set to 0.001 s (equivalent to a sampling frequency f_s = 1000 Hz).

The several driving forces *F(t)* were applied along the y-axis at a height z = 3.87 m, which means assuming a shaker applied at 13 cm from the free end on the central node of the cross-section. The direction of the input was chosen parallel to the crack propagation to have a predominant mode I type of crack opening and a prevalent bending behaviour exciting the breathing mechanism. The dynamic response was computed at 13 cm from the free end (CH1, *top node* in Figure 1), coincident to the hypothetic shaker location. Another channel, located at 25 cm from the fixed end (CH2, *bottom node* in Figure 1), was also used; however, being this latter one farther from the driving force and closer to the restrained extremity, its output was considerably lower, as expected. Since neural networks trained on data recorder at CH2 provided only unsatisfactory results, they have been discarded and not reported here. It is also important to state the beneficial consequences that this implies. Since bispectrum is estimated only at one channel – being it CH1, CH2 or any other location – that means that damage localisation can be performed with just one sensor, rather than an array of them, as it is common for other SHM techniques.

A Rayleigh damped model was assumed. The Rayleigh damping coefficients were computed using the first two bending frequencies (7.06 Hz and 43.83 Hz) with the well-known Rayleigh relationship, assuming both modes have a viscous damping coefficient of the 5% :

$$\begin{cases} \alpha = \zeta\dfrac{2\omega_1\omega_2}{\omega_1+\omega_2} = 3.82 \\ \beta = \zeta\dfrac{2}{\omega_1+\omega_2} = 0.000313 \end{cases} \quad (5)$$

To improve the efficacy of the bispectral-based damage localisation technique through neural networks, a set of input data to feed the network had to be created. Thus, a set of forty different driving forces randomly generated with MatLab was applied to the same node of the SOLID185 model (the previously defined *shaker location*). These 40 inputs will be referred from here onward as to WN1, WN2, etc. up to WN40. All of these have a duration of 100 seconds and a useful sampling frequency of 100 Hz and a variance of the amplitude of ±5 kN. This was intended to excite all the natural frequencies in the range of interest at once, rather than focusing on only one of the computed flexural frequencies. The FE model parameters are set equal

as in the previous section. All these forces generated 40 recorded time-histories at CH1 and as many at CH2.

4. Bispectral features

The bispectra have been computed using the HOSA toolbox for MatLab (Rao & Gabr, 1984)(Niakis & Raghuveer, 1987), between the two variable of integrations f_1 and f_2. Once these higher-order spectra have been plotted on the f_1 - f_2 plane, it becomes easy to exploit phase information (Figure 3).

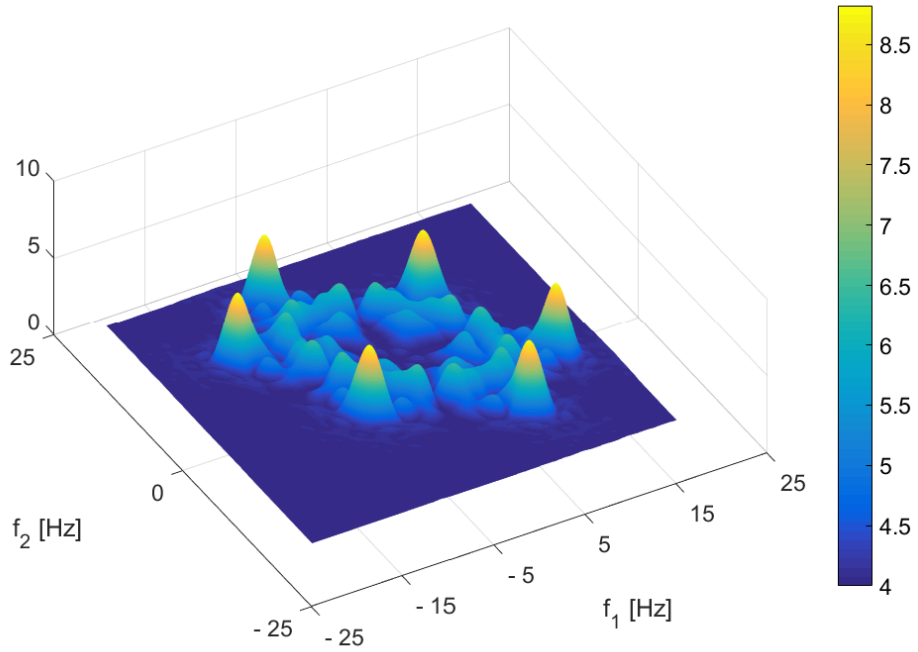

Figure 3. Example of bispectrum obtained from FE numerical simulations. (crack modelled at z = 1.00 m from clamped end).

The peaks indicate the *quadratic phase coupling* (QPC), defined as the pairing of frequency components within a signal, i.e. the coupling at sum and differences of the two frequencies f_1 and f_2. They result from the interaction with some non-symmetric, non-linear mechanisms inside the measured system. So, the amplitude of plotted peaks gives a measure of the level of coupling and then of the amount of non-linearity. Whilst other form of spectra (i.e. power spectrum or autocorrelation function) are "phase blind", higher order spectra make possible detecting and quantifying this nonlinearity in signals (Kicinski & Szczepanski, 2004). In signal processing it is possible to find QPC quite often, where two harmonic signals are processed by a nonlinear system. Let us consider a signal x(t):

$$x(t) = A_1 \cos(\omega_1 t + \phi_1) + A_2 \cos(\omega_2 t + \phi_2) \quad (6)$$

which is given as input to a simple quadratic nonlinear system:

$$y(t) = a \cdot x^2(t) \quad (7)$$

where a is a non-zero constant. The output $y(t)$ of the system will be including the harmonic components: ($2\omega_1$, $2\phi_1$), ($2\omega_2$, $2\phi_2$), ($\omega_1 + \omega_2$, $\phi_1 + \phi_2$) and ($\omega_1 - \omega_2$, $\phi_1 - \phi_2$). This phenomenon is the so-called quadratic phase coupling or phase coupling of the second order. In such a case a power spectrum would show the peaks on the same positions (of the frequencies) independently of the phases of the sinusoids, losing the phase information. This is not the case for higher order spectra. Generally speaking, if a signal is composed of three sinusoids, with frequencies and phases (ω_1, ϕ_1), (ω_2, ϕ_2) and (ω_3, ϕ_3) respectively, then it is possible to define the sinusoids 1 and 2 if and only if $\omega_1 + \omega_2 = \omega_3$ and $\phi_1 + \phi_2 = \phi_3$. In general, a harmonic signal can be composed of k complex sinusoids and defined as:

$$x(t) = \sum_{i=1}^{k} A_i \exp\left(j(\omega_i t + \phi_i)\right) \quad (8)$$

It is possible to determine how many possible different phase couple pairs can appear in such a signal. Let assume as s the number of sinusoids coupled to itself, and p as the total number of unordered pairs of sinusoids in the signal. Consequently, the total number of order pairs is $2p$, whereas the number of different ordered pairs is $2p$-s. It is possible to obtain the differently ordered QPC pairs as $\omega_{1,i} + \omega_{2,i} = \omega_{3,i}$ and $\phi_{1,i} + \phi_{2,i} = \phi_{3,i}$ where $1 \leq i \leq 2p$-s. It is then

possible to write the third order cumulants of the signal x(*t*) according to Swami and Mendel (Swami & Mendel, 1988) as:

$$c_3^x(\tau_1,\tau_2)=\sum_{i=1}^{q}\alpha_i \exp\left(j\left(\omega_{1,i}\tau_1+\omega_{2,i}\tau_2\right)\right) \quad (9)$$

Where q is the number of differently ordered coupled sinusoids present in x(t). It is worth noticing that in equation (9), only the phase-coupled sinusoids appear. This leads to the observation that the bispectrum function is a useful tool for the detection of QPC.

The bispectrum function has been implemented in MatLab® environment by using the aforementioned HOSA toolbox. The toolbox adds several functions dedicated to the various aspects of Higher-Order Statistics, as polispectral estimation for both linear and nonlinear systems. In particular, bispectrum could be computed indirectly (function bispeci(·)) or directly (function bispecd(·)). The main difference is that direct estimation is based on the Fourier transforms of the observed data (inputs), while indirect approach relies on Fourier Transforms of the estimated autocorrelation sequence of the data. For this study, all the bispectra have been estimated by the direct method, also known as the Fast Fourier Transform (FFT)–based technique. Even if the function bispecd(·) was partially rewritten and modified to better fit this research's purposes, computational details remain similar to the original toolbox. The computation of the bispectrum involves four main subsequent steps. Firstly, the given input – the time-series x(t) – is decomposed into several records $x_i(t)$, where i=1, …, K and K depends on the chosen overlap between subsequent windows and of the value of samples for each signal segment. Then, every one of these segments undergoes separately the Fourier transform to $X_i(f)$. At this point, simple triple product is computed as $X_i(f_1)\cdot X_i(f_2)\cdot X_i^*(f_1+f_2)$. Finally, results are averaged across the set of records and smoothed on the frequency domain. In this study the bispectra have been computed using an overlap of 90%, resorting to Rao-Gabr bispectral window.

Having defined the bispectrum itself, firstly a comparison was carried out, in order to spot at first glance the main differences that can occur when crack location is switched (Figure 4), in this case by considering the Absolute component of the complex data. The FFT length was set to 512, since the resolution proved to be good enough while bigger values would have generated too big, unmanageable dataset; in fact, once unrolled in a single-row vector, 512-by-512 bispectra have 262144 elements, and 2048-by-2048 bispectra have 4194304 elements.

The comparison between the pictures in Figure 4 highlights the effects of different crack positions on the analysed signal. These differences are correlated to different displacements recorded at CH1 and ultimately to a variation of the fissure location.

A second useful comparison has been done by comparing the bispectra computed from different driving forces for the same crack position (Figure 5). In the given example, the magnitude of the bispectrum is shown as a contour plot for some random input noise – WN2, 12, 24 and 38 – when the damage is located at x=2.00 m (corresponding to position #5). Even if not identical, the obtained bispectral data show similar bifrequency features, which are characteristic of the specific position of the damage and thus rendering the bispectrum a suitable feature for damage classification.

To further reduce the amount of data to be feed-forwarded to the NN, it is worth to highlight that not the whole bispectrum contains unique information. In fact, third-order moments have six symmetry regions (as it may be clearly observed from Figure 6) and an hexagonal region of integration (Niakis & Raghuveer, 1987) . Moreover, due to the Nyquist criterion and on the presence of the third component $X^*(f_1+f_2)$, only half of the domain of the transform is meaningful.

It is possible to consider the graph as subdivided into its four quadrants, in which (departing from the upper right and moving clockwise) the variables of integration f_1 and f_2 assume the following signs, respectively: (+, +), (+, -), (-, -) and (-, +). In order to interpret the bispectrum, one has to take into account that the FFTs are specular to the axis passing through zero. This means that $X(f_1)$ will be symmetric respect to the y-axis, while $X(f_2)$ respect to the x-axis. This is important because the product of the two, then amplified by $X^*(f_1+f_2)$, defines the bispectrum at any point. As can easily be noticed, the domain is defined by three axes of symmetry, which divide the transform in six zones. These lines $f_1 = 0$, $f_2 = 0$, and $f_1 + f_2 = 0$, are also known as the *principal submanifolds* of the domain (Brillinger & Rosenblatt, 1967). It should also be remembered that this spectrum is obtained as the product of three distinct Fourier transforms (1). Of these, the third component $X^*(f_1+f_2)$ is the one dealing with the non-linear phase coupling in the response. As can be seen, the damaged case is clearly distinct by a peak on the internal bisector of the first region of symmetry; more generally, this happens along all the bisector lines of each one of the six non-redundant zones. That means that the peak in region I has co-ordinates (f_{peak}, f_{peak}), where f_{peak} is not identical to the resonance frequency for the linear case but close to.

One should not be misled by the super- and sub-harmonics lookalike effects appearing on Figure 6. Indeed, these are not true signs of nonlinearity, but most probably due to the numerical computations performed by the software, as $X^*(f_1+f_2)$, which should be null, is never truly zeroed by the code. These numerical imprecisions are visible there since the run data were noise-free, but they become negligible and no more noticeable when noise is added to the signal.

In order to detect the location of damage, it was chosen to follow an approach similar to previous attempts in damage detection/classification (Xiang & Tso, 2002) using one-sixth of the bispectra domain as a feature (Figure 6.b). This should help the training of the NN reducing the dimension of the input to the minimum possible without any other pre-processing.

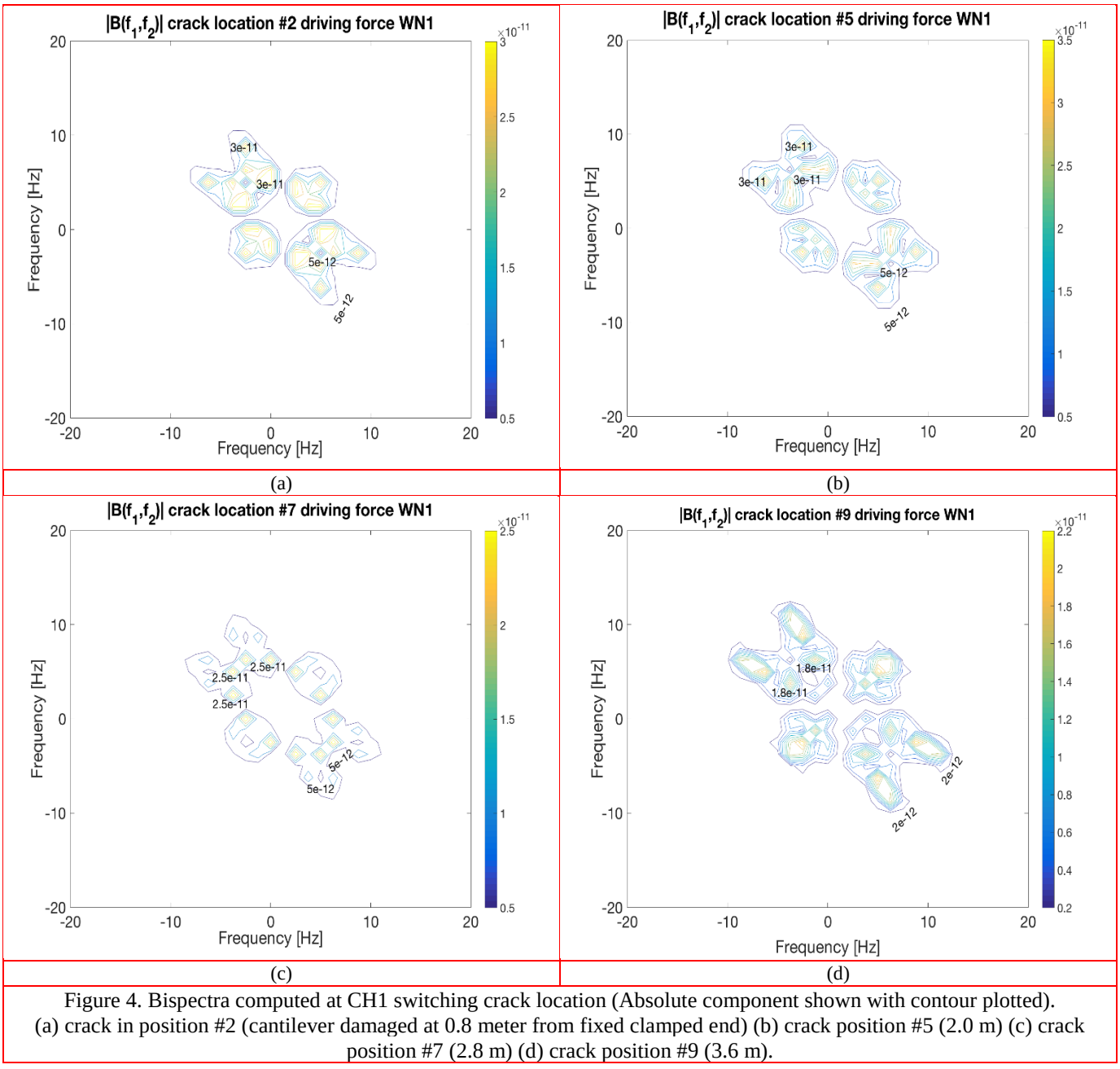

Figure 4. Bispectra computed at CH1 switching crack location (Absolute component shown with contour plotted). (a) crack in position #2 (cantilever damaged at 0.8 meter from fixed clamped end) (b) crack position #5 (2.0 m) (c) crack position #7 (2.8 m) (d) crack position #9 (3.6 m).

Furthermore, it was also noticed that the useful information is not equally distributed among the whole selected, triangular area. As can be easily noticed by looking at Figure 6.b, the helpful bispectral data are mostly clustered; even if blank zones in a contour plot are not necessarily an indicator of null or someway unneeded data, it was tested that running the NN training over a much-restricted amount of inputs (corresponding to the pixels closer to the centre of the bispectra) both accelerated and ameliorated the training process. Hence, only 1256 of the 8256 elements included in the vector of unrolled data has been used, as indicated in Figure 7.

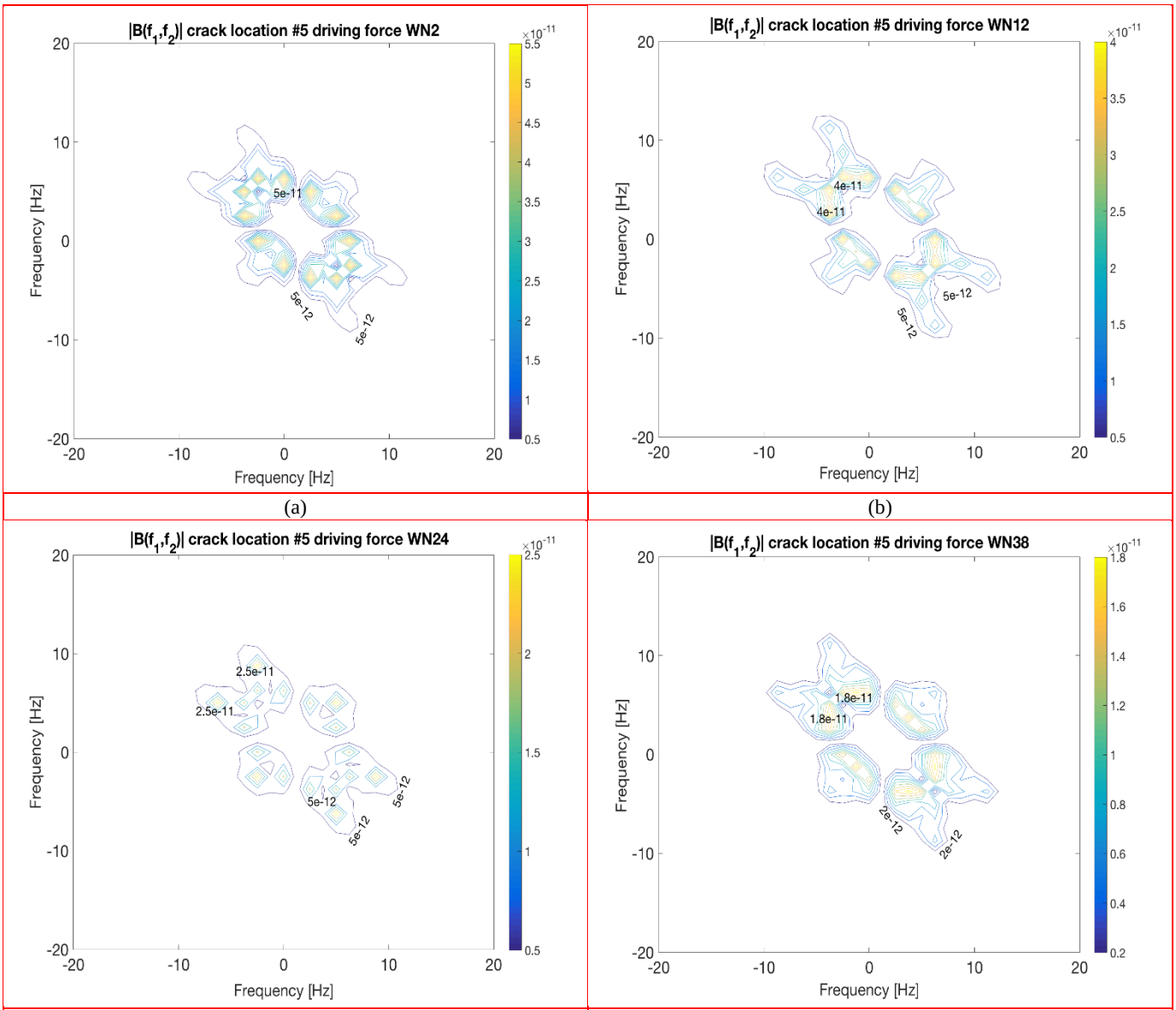

Figure 2. Bispectra computed at CH1 using different driving force (absolute component shown). From top left: (a) WN #2, (b) WN #12, (c) WN #24 and (d) WN #38. For all cases, the damaged cross-section was set at x=2.00 (position #5).

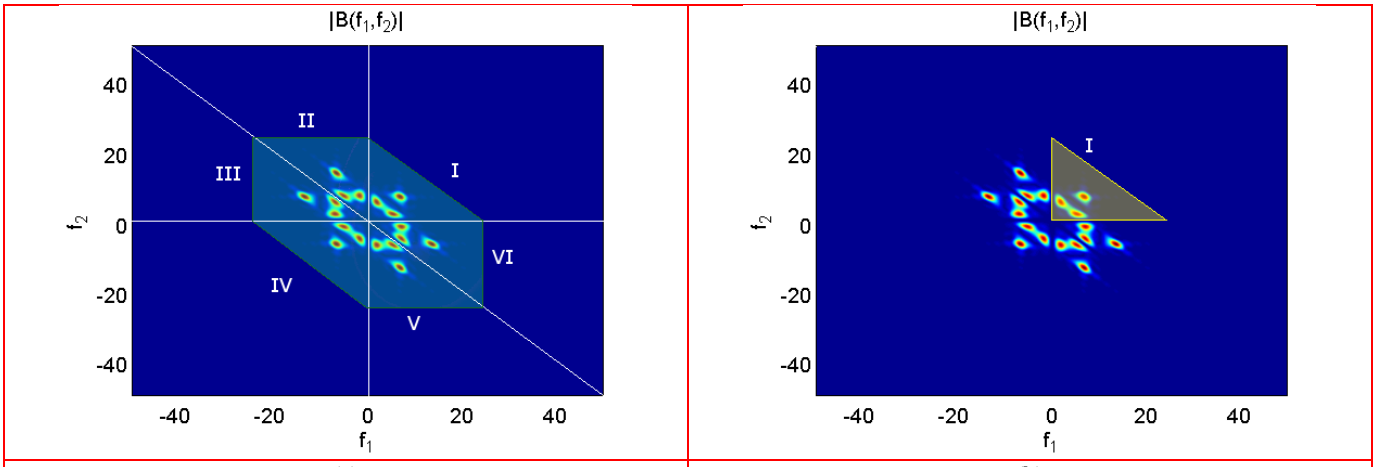

Figure 6. (a) symmetry regions of third-order moment with the useful domain highlighted (b) triangular feature selected in region I (8256 elements inside) for training.

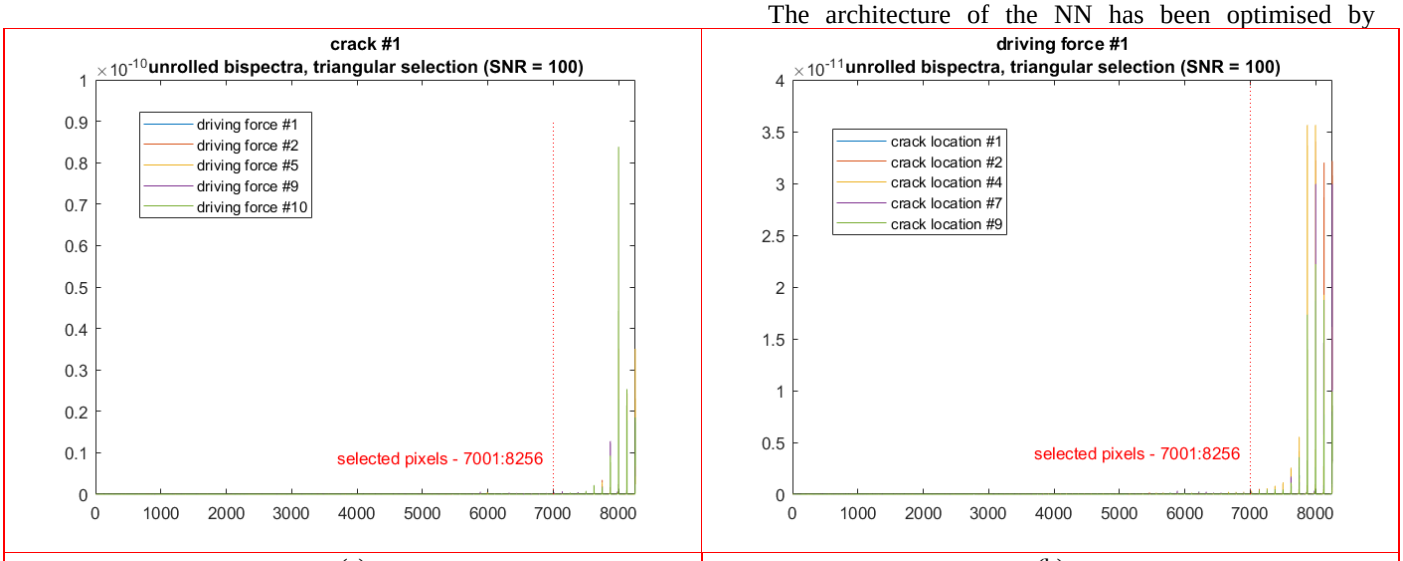

(a) (b)

Figure 7. Examples of elements inside the various vectors of unrolled bispectrum (triangular selection, region I; bispectra considered: (a) five different driving forces applied with the same crack location (b) five different crack locations under the same driving force). Red dotted vertical line represents the lower bound of the selected pixels.

5. Neural Network architecture optimisation and training

The NN has been trained until it proved itself able to identify the crack location between the nine possibilities defined (z = 0.4, 0.8, 1.2, 1.6, 2.0, 2.4, 2.8, 3.2 and 3.6 m from the fixed end location and moving towards the free extremity). The overall plan of simulations was to compute the bispectra for 40 white Gaussian noise input with the crack located in one of these 9 different locations. In order to have a dataset large enough to train the NN, 5 samples for each case were generated by adding white Gaussian noise (SNR=100, 50 or 20) to the structural response at the free and the clamped end locations (in terms of displacements). This lead to the definition of 1800 bispectra from CH1– or five times forty driving forces, each one computed nine times by switching the crack position.

Out of the 40 driving forces, 30 independent cases have been used for the training set, 5 for the validation set at 5 for the test set. The simulations were carried out on the High Performance Computing (HPC) systems Grid and Delta of Cranfield University, so to parallelise the computing procedures (two Linux clusters with 284 and 1920 CPU cores, respectively). It is important to state that statistical validation is inherently a strong approach, much stricter than others such as cross-validation. Indeed, the proposed approach considered three perfectly distinct sets for training, validation and test. Differently from cross-validation, where all observations are divided into several subsets that are, from time to time, used for training, validation and testing, here the observations used for validation have never been seen before by the Machine. That means that the driving forces used to validate results are completely new and different; this proof the ANN ability to recognise a known case (i.e. a crack in a given location) in a never-seen-before condition (i.e. a completely novel state of external excitation).

The architecture of the NN has been optimised by varying the number of neurons on its hidden layer between 10 and 50, in steps of two by two. A bias unity is added to the hidden layer. A final (output) layer was composed by the nine possible locations to be predicted (Figure 8).

Regarding to the number of hidden layer implemented, the default option was to have one. In fact, according to the universal approximation theorem (Hornik, Stinchcombe, & White, 1989), an Artificial NN with a single hidden layer with a finite number of neurons can approximate continuous functions on compact subsets of $\mathbb{R}^n$. In other words, the simplest possible NN should be able to represent a great number of possibly useful functions; that is to say, there is no reason to suppose a more complex architecture – i.e., to resort to Deep Learning techniques – at the beginning, if no specific motivation arises. The same, further training were conducted on NNs with two hidden layers, by changing the number of nodes per hidden layer but maintaining the same amount identical for both layers – i.e., $S_1 = S_2$. However, since no promising improvements have been detected in doing so, while on the other hand the process became noticeably more time-consuming and computationally expensive, this option has been discarded and results related to it are not reported here.

The decision to stop the investigation at 50 nodes per hidden layer is mainly due to preliminary studies performed on the NN architecture accordingly to the considered performance parameter, the aggregate Cross-Entropy (CE), which behaved better – i.e., decreased – along this range.

Notoriously, Cross-Entropy strongly penalise extremely inaccurate outputs, while is less harsh for tolerable mismatches; thus, it is considered to be a very good performance indicator for classifiers operating with discrete output, as the Mean Square Error is for regression with continuous output.

The training was performed minimising the regularised cost function (10) where the indices represent respectively: m is the number of training examples, K is number of final output (9 zones of classification), N is the number of layers,

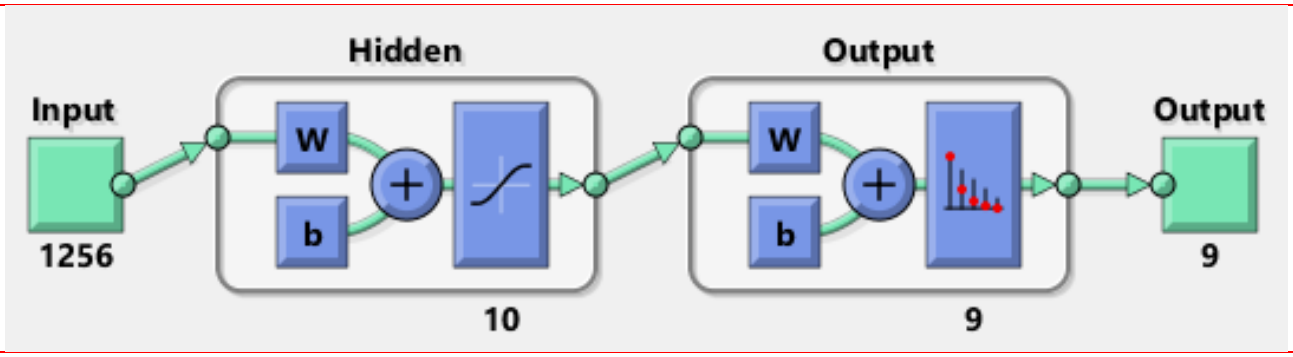

Figure 8. Simplified architecture of the 10 neurons-per-hidden-layer Neural Network. The input layer is of 1256 neurons in 4 cases (Re, Imm, Abs and Angle) and of 2512 neurons in 2 cases (Re-Imm, Abs-Angle). Hidden layer size has been varied ranging from 10 to 50 nodes (in steps of 2) to find the optimal configuration.

S_i and S_o are the input and output number of neurons for each regularisation layer, and θs are actually the weights assigned to the feature (in this particular case, bispectral data) which is used in training; their optimisation is *the* aim of the ML algorithm, which is required to produce an ensemble of thetas that will make the hypothesis function fit the training set well.

$$J(\theta) = \frac{\lambda}{m}\sum_{i=1}^{m}\sum_{k=1}^{K}\left[-y_k^{(i)} \cdot \ln\left(h_\theta\left(x^{(i)}\right)\right)_k\right] + \frac{(1-\lambda)}{2m}\left[\sum_{n=1}^{N-1}\sum_{j=1}^{So}\sum_{k=1}^{Si}\left(\Theta_{j,k}^{(n)}\right)^2\right] \quad (10)$$

Moreover, $y_k^{(i)}$ and $\ln\left(h_\theta\left(x^{(i)}\right)\right)_k$ are, respectively, the expected target value and the natural logarithm of the predicted output for the specific case *i*, *k*.

The factor λ is called performance ratio and causes the network to have smaller weights and biases, thus leading the NN response to be smoother and less likely to overfit. The residual error is defined in term of the aforementioned Cross-Entropy, and is the first term of the cost function, whilst the second part is referred to the regularisation terms. The core of this additional part is the matrix of all weights, capital Theta (Θ), defined separately for each layer according to the number of input nodes (from the previous *n -1*-th layer) and to the number of output destinations (in a similar fashion, considering the *n + 1*-th layer).

As mentioned before, the idea is to train the NN using the feature extracted from the bispectra and then further selected (Figure 6.b, 7.a and 7.b), analysing six different bispectra components, since being the bispectrum a matrix of complex numbers, it is possible to analyse different component data for the bispectrum (modulus, phase, real part or imaginary component). Two further cases are trained combining real plus imaginary case and magnitude plus phase. Totally, 18 cases have been analysed, using three different levels of SNR in the bispectra (100, corresponding to low noise, 50, medium noise, 20, high noise).

For each of these cases, several trainings using the data generated at the free end channel CH1 were carried out using the NN depicted in Figure 8. In fact, Eq. (10) was minimised assuming different values of the regularisation factor λ, thus allowing the maximisation of the predictive capabilities of the NN. The parameter λ was studied in a logarithmic-like fashion, considering the following 7 values: .001, .0033, .01, .0333, .1, .3333 and .9. The value of this parameter cannot be known a priori and it is strongly influenced by the cost function and the NN architecture. Typically, low value of λ can lead to overfitting the penalty function, thus reducing the generalisation capability of the NN, whilst high value of λ may render the cost function insensitive to the optimisation procedure.

The optimisation algorithm used for the minimisation of (10) is based on the gradient descent method and the Polack-Ribiere flavour of conjugate gradients to compute the search directions. Line search using quadratic and cubic polynomial approximations and the Wolfe-Powell stopping criteria is used together with the slope ratio method for guessing the initial step sizes. For the sake of this study, a maximum limit on the training epochs was set equal to 1000. Moreover, a truncation tolerance was set on the minimum gradient variation at 1e-10. For what concerns the convergence criterion, it was set equal to 0.

6. Neural networks and feature performance

The NNs trained using the feature module (absolute value – Abs(z)) of the bispectrum have performed better than most of the other components. Also the real part generally led to NNs performances slightly better than imaginary or phase (see Table 2). In particular, for SNR = 100, magnitude-trained NNs clearly outperformed the other neural networks fed with any other feature extracted by the same bispectra. Thus, the absolute value seemed to be the most sensitive feature to changes in damage location. The combination of real and imaginary part, or of module and phase, led to performances of the NNs similar to the one using only the real part or the module – that is to say, with no noticeable gain. On the other hand, combining Abs and Angle features seemed to improve results, yet only for high level of noise (SNR = 20), whilst being eventually detrimental for less noise-affected signals. This seems to indicate that magnitude and phase are more robust, whilst

the module is much more affected and proves to be the most apt feature to classify the position of the damage overall.

Table 2 shows the average performance in term of CE for different noise levels. It is possible to see that the overall CE minimum roughly doubles from SNR=100 to SNR=50 (green-highlighted boxes).

Table 2 Results summary with respect to different cases and features.

Bispectra Component	**Aggregate Cross-Entropy Residual on Test Set**								
	SNR 20			**SNR 50**			**SNR 100**		
	min	**max**	**μ**	**min**	**max**	**μ**	**min**	**max**	**μ**
Real Part (Re)	0.0285	0.3135	0.2233	0.0287	0.2880	0.2164	0.0241	1.20e+06	9.64e +03
Imaginary Part (Im)	0.0291	0.3003	0.2210	0.0285	0.3061	0.2188	0.0247	4.78e+06	3.25e +04
Magnitude (Abs)	0.0285	0.2602	0.2033	0.0183	0.2433	0.1333	0.0107	6.37e+06	5.41e +04
Phase (Angle)	0.0324	0.4294	0.2831	0.0333	0.4627	0.2927	0.0298	0.42e+06	0.27e +03
Real and Imaginary	0.0275	0.3051	0.2228	0.0276	0.2907	0.2174	0.0250	2.29e+09	1.57e +07
Magnitude and Phase	0.0269	0.2888	0.2133	0.0217	0.2502	0.0276	0.0235	3.92e+07	4.83e +05

Most Sensitive Feature	**Optimal NN Architecture**					
	Hidden Layer Size	**Regularisation Factor λ**	**Hidden Layer Size**	**Regularisation Factor λ**	**Hidden Layer Size**	**Regularisation Factor λ**
SNR = 50 and 100: Magnitude (Abs); SNR = 20: Magnitude and Phase	22	0.9000	26	0.9000	26	0.9000

Finally, the confusion matrices for the best NN trained are depicted in Figure 9. As it is possible to see, the accuracy on the test-set is 71% circa, while all-around accuracy on the three sets (Training, Validation and Test) is 80%. It is worth to remember that the validation and the test set were chosen amongst white Gaussian noise different from the ones used in the training set, therefore are data completely new for the trained NN. The best performance was achieved with a 26 neurons NN with a regularisation factor of 0.9000.

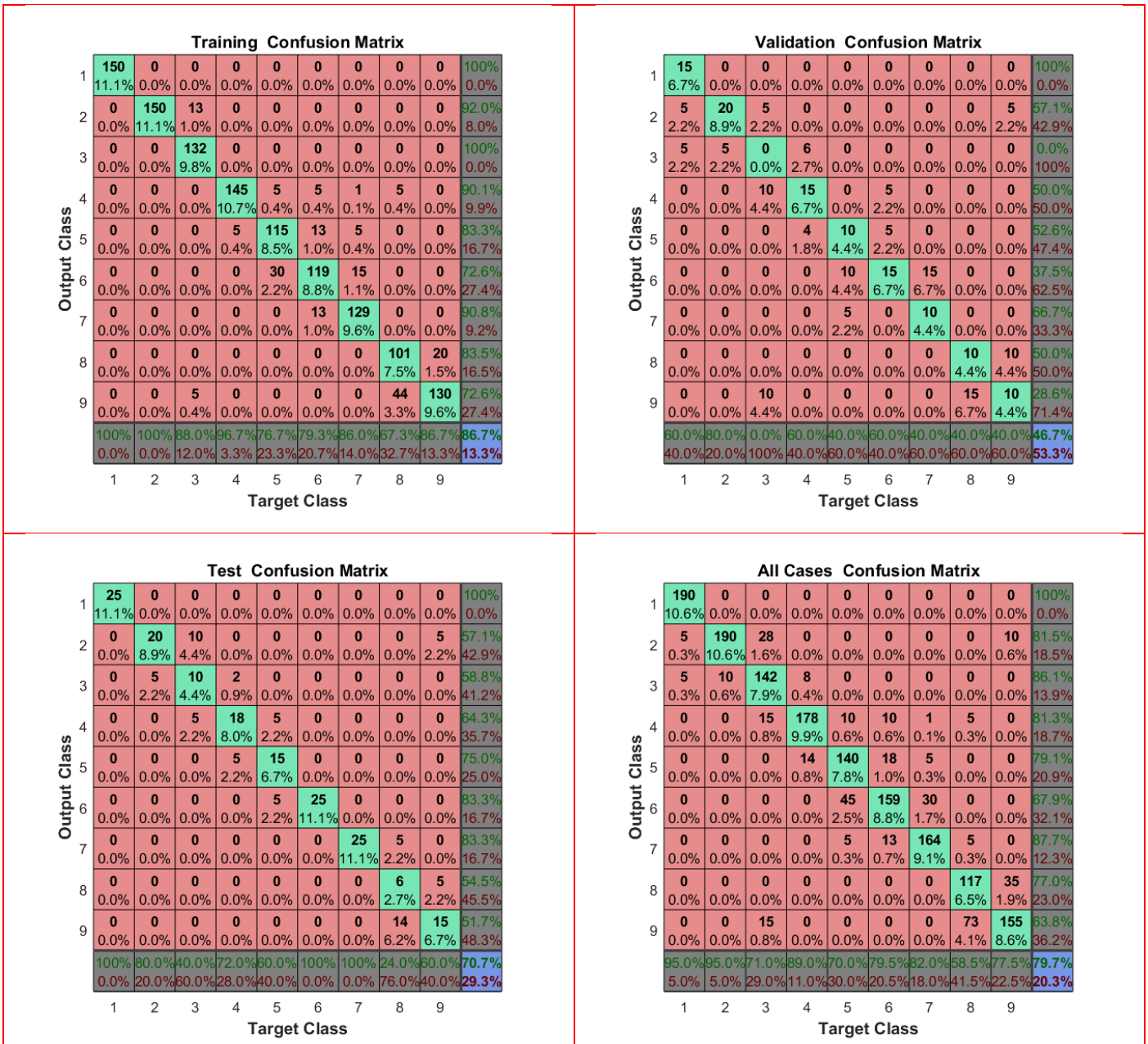

Figure 9. Confusion matrix for the best NN trained (SNR = 100): using Abs component, 26 Neurons and λ=0.9000

7. Test on cracks located into intermediate positions

Since the ANN has been trained for classification between a finite number of possible locations (the nine positions described before), the possibility of cracks located in intermediate positions has been investigated, in order to test the Machine ability to manage cases close to but not exactly located into their possible outputs.

Only the best-trained NNs (for SNR = 100 and SNR = 50) has been tested so. By using the same FE model of a beam, a set of six intermediate cracks has been realised, located at 0.3, 0.9, 1.9, 2.9, 3.5 and 3.7 meters from the fixed end. The set was so composed in order to be representative of the three main regions of the beam – fixed end, free end, and mid-length. Indeed, the first two cases represent the immediate surroundings of crack location #1 (z = 0.4 m) and #2 (z = 0.8 m). Third and four cases, similarly, are close to the crack location #5 (z = 2.0 m) and #7 (z = 2.8 m) respectively. Finally, the latter two configurations encircle crack location #9 (z = 3.6); crack location #8 (z = 3.2 m) neighbours these two from one side, while the beam free end bounds them from the other.

Ten different driving forces were newly generated for the task, similarly to the previous ones used for training and validation; they were named, accordingly, WN41 to WN50, and applied separately to each new crack investigated. Thus, sixty new bispectra were computed.

Since the 26-neurons-per-hidden-layer NN (for signal-to-noise ratio equal to 100) performed remarkably well for locations closest to the fixed edge, it was expected to see a major accuracy for the first elements of this set; this prevision has been proved right by the results of the NN.

Effectively, the NN seems to suffer to recognise distinct mid-length cracks (Figure 10); however, locations closest to the actual intermediate cracks remain in all cases the most recurring outputs, hence the most statistically probable; even when not correct, predictions are always not far from the expected results. For instance, it is shown in Figure 10.a how, out of 10 inputs related to crack at z = 1.9 m, seven where correctly located at crack location #5 (2.0 m), one at #4 (1.6 m, second closest target) and two at #6 (2.4 m, third closest). Similar conclusions can be drawn by the results related to the remaining intermediate cracks. Largest error occurred for the crack pair z = 3.5 and 3.7, which were spotted correctly 13 times out of 20, with a minimal error 5 times, but went evidently wrong twice. Results from SNR = 50 (Figure 10.b) suffered noticeably from the higher noise level, but the same behaviour can be noticed – erroneous locations tend to be not far from closest, expected outputs.

These validating results can be seen as a further proof that cracks in different positions generate variations in the bispectra of the recorder displacements and that this features can be used for localisation through Machine Learning, with an output-only approach.

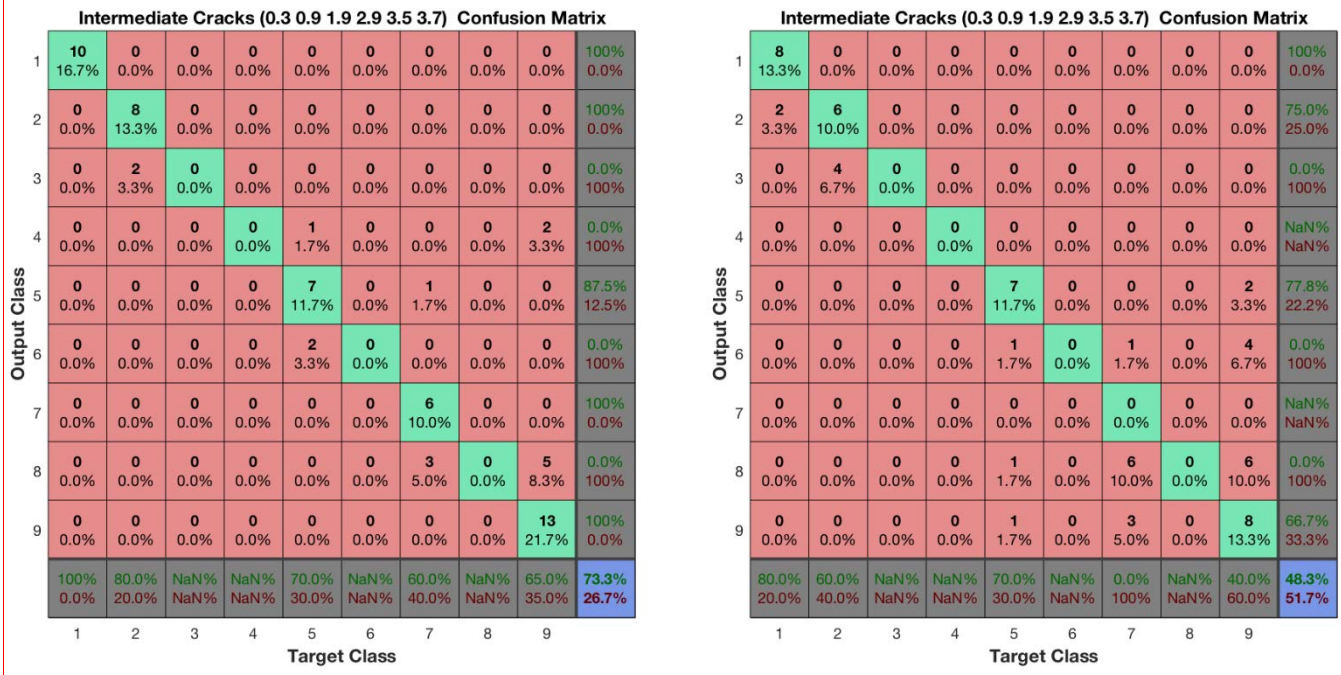

(a) (b)

Figure 10. (a) Confusion matrix, SNR = 100; (b) Confusion matrix, SNR = 50; selected feature: absolute values of bispectral data (for both cases). Closest targets: crack location #1 for z = 0.3 m; #2 for z = 0.9 m; #5 for z = 1.9 m; #7 for z = 2.9 m; and #9 for both z = 3.5 m and z = 3.7 m.

8. Conclusions

The main objective of this work is a feasibility study on using bispectrum as a mean of damage localisation, knowing that the bispectrum and bicoherence has been already proved as good damage indicators. At this aim, several NN architectures and configurations were trained and validated, feeding them with data achieved by running various simulations on FE models excited by randomly generated driving forces.

In conclusion, the main results of the present paper can be summarised as follows:

- Bispectrum proved to be a suitable technique for damage localisation, since by varying the crack position, and using state-of-the-art techniques for multi-classification problems, it was possible to extract features from the bispectra able to detect these changes (i.e. within the 10% of the length of the beam);
- Out of all the investigated combinations – component of the complex numbers and settings of the NNs – resulted quite clearly that: (1) the module is the most sensitive features for damage localisation (2) the combination of the real part and of the module with their complex counterparts, imaginary part and the phase, did not lead to significant improvements in the NN performance, even if it can turns out to be more robust for higher noise levels. (3) it was already known from previous studies that considering the whole bispectrum is redundant and not efficient. Indeed, here an accuracy on the test-set of approximately 71% has been reached with just 1256 carefully chosen elements (out of the 262144 included into the 512-by-512 dataset matrices).
- The best performing NN was composed of one hidden layer of 26 neurons and reached a promising

overall accuracy around 80 % with a training set of 1500 cases.

There are future perspectives that are worth to be investigated in order to improve the reliability of the method. In fact, now that a link between the bispectrum properties and the damage localisation has been established, a more in-depth study about the intrinsic properties of the non-linear response can lead to a more focused feature extraction that may help in the damage localisation problem. Currently, the sensitivity of the technique to damage severity is also being investigated in an ongoing research; furthermore, future studies may involve different excitation sources, to study the beam dynamic close to resonance and possibly expand the results with an experimental specimen.

If successful, the proposed method will have undoubted practical advantages, such as the need or only one sensor, an output-only data-based approach, an adaptability to different shapes and sizes of various structures (if properly trained on them), and more.

Acknowledgments

The authors wish to thank Cranfield University for the facilities provided and Politecnico di Torino for having allowed this joint research work.

References

Akan, A., & Ünsal Artan, R. B., (2003), "Time-varying bispectral analysis of nonstationary signals",In *Proceedings - 7th International Symposium on Signal Processing and Its Applications, ISSPA 2003* (Vol. 1, pp. 569–572), IEEE. http://doi.org/10.1109/ISSPA.2003.1224767

Bathe, K.-J., (2005), *Finite Element Procedures*, Prentice Hall, London.

Belytschko, T., Liu, W. K., Moran, B., & Elkhodary, K., (2013), *Nonlinear Finite Elements for Continua and Structures* (Vol. 2013), John Wiley & Sons, Chichester, UK.

Boscato, G., Russo, S., Ceravolo, R., & Zanotti Fragonara, L., (2015), "Global Sensitivity-Based Model Updating for Heritage Structures", *Computer-Aided Civil and Infrastructure Engineering*, **30**(8), 620–635. http://doi.org/10.1111/mice.12138

Bovsunovsky, A. P., & Surace, C., (2005), "Considerations regarding superharmonic vibrations of a cracked beam and the variation in damping caused by the presence of the crack", *Journal of Sound and Vibration*, **288**(4–5), 865–886. http://doi.org/10.1016/j.jsv.2005.01.038

Bovsunovsky, A. P., Surace, C., & Bovsunovsky, O. A., (2006), "The effect of damping and force application point on the non-linear dynamic behavior of a cracked beam at sub- and superresonance vibrations", *Strength of Materials*, **38**(5), 492–497. http://doi.org/10.1007/s11223-006-0068-8

Bovsunovsky, A., & Surace, C., (2015, October), "Non-linearities in the vibrations of elastic structures with a closing crack: A state of the art review", *Mechanical Systems and Signal Processing*. http://doi.org/10.1016/j.ymssp.2015.01.021

Brillinger, D. R., & Rosenblatt, M., (1967), "Asymptotic theory of estimates of kth-order spectra", *Proceedings of the National Academy of Sciences of the United States of America*, **57**(2), 206–210. Retrieved from http://www.pubmedcentral.nih.gov/articlerender.fcgi?artid=335489&tool=pmcentrez&rendertype=abstract

Chandrashekhara, K., & Bangera, K. M., (1993), "Linear and geometrically non-linear analysis of composite beams under transverse loading", *Composites Science and Technology*, **47**(4), 339–347. http://doi.org/10.1016/0266-3538(93)90003-Y

Chati, M., Rand, R., & Mukherjee, S., (1997), "Modal Analysis of a Cracked Beam", *Journal of Sound and Vibration*, **207**(2), 249–270. http://doi.org/10.1006/jsvi.1997.1099

Chen, J., Hagiwara, I., Su, X., & Shi, Q., (2002), "A Bispectrum Feature Extraction Enhanced Structure Damage Detection Approach.", *JSME International Journal Series C*, **45**(1), 121–126. http://doi.org/10.1299/jsmec.45.121

Chondros, T. G., Dimarogonas, A. D., & Yao, J., (1998), "Longitudinal vibration of a bar with a breathing crack", *Engineering Fracture Mechanics*, **61**(5–6), 503–518. http://doi.org/10.1016/S0013-7944(98)00077-0

Ciang, C. C., Lee, J.-R., & Bang, H.-J., (2008), "Structural health monitoring for a wind turbine system: a review of damage detection methods", *Measurement Science and Technology*, **19**(12), 122001. http://doi.org/10.1088/0957-0233/19/12/122001

Civera, M., Surace, C., & Worden, K., (2017), "Detection of Cracks in Beams Using Treed Gaussian Processes", *Structural Health Monitoring & Damage Detection, Vol. 7. Conference Proceedings of the Society for Experimental Mechanical Series* ,85–97. http://doi.org/10.1007/978-3-319-54109-9_10

Civera, M., Zanotti Fragonara, L., & Surace, C., (2016), "Using Bispectral Analysis and Neural Networks To Localise Cracks in Beam-Like Structures",In *8th European Workshop On Structural Health Monitoring (EWSHM 2016), 5-8 July 2016, Spain, Bilbao*, Bilbao. Retrieved from http://www.ndt.net/events/EWSHM2016/app/content/Paper/68_Civera.pdf

Collis, W. B., White, P. R., & Hammond, J. K., (1998), "Higher-Order Spectra: the Bispectrum and Trispectrum", *Mechanical Systems and Signal Processing*, **12**(3), 375–394. http://doi.org/10.1006/mssp.1997.0145

Fackrell, J., (1995), "The interpretation of the bispectra of vibration signals— II. Experimental results and applications", *Mechanical Systems and Signal Processing*, **9**(3), 267–274. http://doi.org/10.1006/mssp.1994.0022

Farrar, C. R., & Worden, K., (2007), "An introduction to structural health monitoring.", *Philosophical Transactions. Series A, Mathematical, Physical, and Engineering Sciences*, **365**(1851), 303–315. http://doi.org/10.1098/rsta.2006.1928

Gerstle, W. H., Martha, L. F., & Ingraffea, A. R., (1987), "Finite and boundary element modeling of crack propagation in two and three dimensions", *Engineering with Computers*, **2**(3), 167–183. http://doi.org/10.1007/BF01201264

Greb, U., & Rusbridge, M. G., (2000), "The interpretation of the bispectrum and bicoherence for non-linear interactions of continuous spectra", *Plasma Physics and Controlled Fusion*, **30**(5), 537–549. http://doi.org/10.1088/0741-3335/30/5/005

Hillis, A. J., & Courtney, C. R. P., (2011), "Structural health monitoring of fixed offshore structures using the bicoherence function of ambient vibration measurements", *Journal of Sound and Vibration*, **330**(6), 1141–1152. http://doi.org/10.1016/j.jsv.2010.09.019

Hillis, A. J., Neild, S. A., Drinkwater, B. W., & Wilcox, P. D., (2006), "Global crack detection using bispectral analysis", *Proceedings of the Royal Society A: Mathematical, Physical and Engineering Sciences*, **462**(2069), 1515–1530. http://doi.org/10.1098/rspa.2005.1620

Hornik, K., Stinchcombe, M., & White, H., (1989), "Multilayer feedforward networks are universal approximators", *Neural Networks*, **2**(5), 359–366. http://doi.org/10.1016/0893-6080(89)90020-8

Kicinski, W., & Szczepanski, A., (2004), "Quadratic Phase Coupling phenomenon and its properties", *Hydroacoustics*, **7**, 97–106.

Kim, J.-T., & Stubbs, N., (2002), "Improved damage identification method based on modal information", *Journal of Sound and Vibration*, **252**(2), 223–238. http://doi.org/10.1006/jsvi.2001.3749

Kim, Y. C., & Powers, E. J., (1978), "Digital bispectral analysis of self-excited fluctuation spectra", *Physics of Fluids*, **21**(1978), 1452. http://doi.org/10.1063/1.862365

Kisa, M., & Gurel, M. A., (2006), "Modal analysis of multi-cracked beams with circular cross section", *Engineering Fracture Mechanics*, **73**(8), 963–977. http://doi.org/10.1016/j.engfracmech.2006.01.002

Macneal, R. H., & Harder, R. L., (1985), "A proposed standard set of problems to test finite element accuracy", *Finite Elements in Analysis and Design*, **1**(1), 3–20. http://doi.org/10.1016/0168-874X(85)90003-4

Martha, L. F., Wawrzynek, P. A., & Ingraffea, A. R., (1993), "Arbitrary crack representation using solid modeling", *Engineering with Computers*, **9**(2), 63–82. http://doi.org/10.1007/BF01199046

Michel, C., Hans, S., Guéguen, P., & Boutin, C., (2007), "In Situ Experiment and Modelling of RC-Structure using Ambient Vibration and Timoshenko Beam",In *Proceedings of 1st European Conference of Earthquake Engineering and Seismology (ECEES) - 1st European Conference of Earthquake Engineering and Seismology (ECEES)*, Geneva, Switzerland.

Niakis, C. L., & Raghuveer, M. R., (1987), "Bispectrum estimation: a digital signal processing framework", *Proc. IEEE*, **75**, 869–891.

Nikias, C. L., & Mendel, J. M., (1993), "Signal processing with higher-order spectra", *IEEE Signal Processing Magazine*, **10**(3), 10–37. http://doi.org/10.1109/79.221324

Pugno, N., Surace, C., & Ruotolo, R., (2000), "Evaluation of the Non-Linear Dynamic Response To Harmonic Excitation of a Beam With Several Breathing Cracks", *Journal of Sound and Vibration*, **235**(5), 749–762. http://doi.org/http://dx.doi.org/10.1006/jsvi.2000.2980

Rao, T. S., & Gabr, M. M., (1984), *An Introduction to Bispectral Analysis and Bilinear Time Series Models* (Vol. 24), Springer US, New York, NY. http://doi.org/10.1007/978-1-4684-6318-7

Roy, T., Kumar, A., & Bahl, R., (2002), "Detection Of Quadratic Phase Coupling In Shallow Underwater Channel", *OCEANS'02 MTS/IEEE*, **4**, 2180–2186. http://doi.org/10.1109/OCEANS.2002.1191968

Ruotolo, R., Surace, C., Crespo, P., & Storer, D., (1996), "Harmonic analysis of the vibrations of a cantilevered beam with a closing crack", *Computers and Structures*, **61**(6), 1057–1074. http://doi.org/10.1016/0045-7949(96)00184-8

Salawu, O. S., (1997), "Detection of structural damage through changes in frequency: a review", *Engineering Structures*, **19**(9), 718–723. http://doi.org/10.1016/S0141-0296(96)00149-6

Sundermeyer, J. N., & Weaver, R. L., (1995), "On crack identification and characterization in a beam by non-linear vibration analysis", *Journal of Sound and Vibration*, **183**(5), 857–871. http://doi.org/10.1006/jsvi.1995.0290

Surace, C., Ruotolo, R., & Storer, D., (2011), "Detecting nonlinear behaviour using the Volterra series to assess damage in beam-like structures", *Journal of Theoretical and Applied Mechanics*, **49**(3), 905–926. Retrieved from http://www.ptmts.org.pl/jtam/index.php/jtam/article/view/v49n3p905

Swami, A., & Mendel, J., (1988), "Adaptive Cumulant-Based Estimation of ARMA Parameters",In *American Control Conference*, 2114–2119. Retrieved from http://ieeexplore.ieee.org/stamp/stamp.jsp?tp=&arnumber=4790073&isnumber=4789672

Xiang, Y., & Tso, S. K., (2002), "Detection and classification of flaws in concrete structure using bispectra and neural networks", *NDT & E International*, **35**(1), 19–27. http://doi.org/10.1016/S0963-8695(01)00018-4

Figure Caption List

Figure 1. Cantilever beam geometry (section 0.2 by 0.2 m, length 4 m) and the two measurements position. The extension of the cracks was assumed to be half the width of the beam. The nine crack locations are all spaced by 40 cm from each other and from the fixed and free ends.

Figure 2. Breathing crack mechanism (crack open during modal analysis). Displacement over-magnified for clarity's sake.

Figure 3. Example of bispectrum obtained from FE numerical simulations (crack modelled at z = 1.00 m from clamped end).

Figure 4. Bispectra computed at CH1 switching crack location (Absolute component shown with contour plotted). (a) crack in position #2 (cantilever damaged at 0.8 meter from fixed clamped end). (b) crack position #5 (2.0 m) (c) crack position #7 (2.8 m) (d) crack position #9 (3.6 m).

Figure 5. Bispectra computed at CH1 using different driving force (absolute component shown). From top left: (a) WN #2, (b) WN #12, (c) WN #24 and (d) WN #38. For all cases, the damaged cross-section was set at x=2.00 (position #5).

Figure 6. (a) symmetry regions of third-order moment with the useful domain highlighted (b) triangular feature selected in region I (8256 elements inside) for training.

Figure 7. Examples of elements inside the various vectors of unrolled bispectrum (triangular selection, region I; bispectra considered: (a) five different driving forces applied with the same crack location (b) five different crack locations under the same driving force).

Figure 8. Simplified architecture of the 10 neurons-per-hidden-layer Neural Network. The input layer is of 1256 neurons in 4 cases (Re, Imm, Abs and Angle) and of 2512 neurons in 2 cases (Re-Imm, Abs-Angle). Hidden layer size has been varied ranging from 10 to 50 nodes (in steps of 2) to find the optimal configuration.

Figure 9. Confusion matrix for the best NN trained (SNR = 100): using Abs component, 26 Neurons and λ=0.9000

Figure 10. (a) Confusion matrix, SNR = 100; (b) Confusion matrix, SNR = 50; selected feature: absolute values of bispectral data (for both cases). Closest targets: crack location #1 for z = 0.3 m; #2 for z = 0.9 m; #5 for z = 1.9 m; #7 for z = 2.9 m; and #9 for both z = 3.5 m and z = 3.7 m.

Table Caption List

Table 1. Modal Analysis results on pristine (undamaged) cantilever beam. All bending modes occur at the same frequency along both directions (x and y axes)

Table 2. Results summary with respect to different cases and features.

2017-12-31

A novel approach to damage localisation based on bispectral analysis and neural network

Civera, M.

Techno Press

M. Civera, L. Zanotti Fragonara, C. Surace. (2017) A novel approach to damage localisation based on bispectral analysis and neural network. Smart Structures and Systems, Volume 20, Issue 6, pp. 669-682

http://dx.doi.org/10.12989/sss.2017.20.6.669